Journal of Electroceramics 4:1, 167–177, 2000

Room Temperature Magnetoresistance at Low Magnetic Fields in $La_{0.7}Ba_{0.3}MnO_3$

M.C. ROBSON, C. KWON,[1] S.E. LOFLAND,[2] S.B. OGALE, S.M. BHAGAT, M. RAJESWARI, T. VENKATESAN[3] & R. RAMESH[4]

Center for Superconductivity Research, Department of Physics, University of Maryland, College Park, MD 20742
E-mail: mrobson@squid.umd.edu

Submitted January 8 1999; Revised September 23, 1999; Accepted September 30, 1999

Abstract. This paper examines the possibility of enhancing the room temperature magnetoresistance at low applied magnetic fields in single layer $La_{0.7}Ba_{0.3}MnO_3$ thin films. The influence of lattice mismatch strain, as well as the effect of different frequency regimes, on the magnetoresistance is explored. The effects of lattice mismatch strain are studied by measuring the magnetoresistance as a function of the $La_{0.7}Ba_{0.3}MnO_3$ film thickness, oxygen annealing, and lattice matched buffer layers. We find that the release of the lattice mismatch strain improves the magnetoresistance at room temperature and at low magnetic fields. In fact, the highest magnetoresistance at room temperature (-1.7% at 500 Oe) has been found for the 1600 Å as-grown $La_{0.7}Ba_{0.3}MnO_3$ film, whereas the largest magnetoresistance (-1.9% at 500 Oe) is found at 309 K for the 1000 Å $La_{0.7}Ba_{0.3}MnO_3$ film annealed in flowing O_2 for 1 h at 900°C. Finally, we find that the microwave magnetoresistance is the same as the dc magnetoresistance when the cavity corrections are applied. In the single layer $La_{0.7}Ba_{0.3}MnO_3$ system, the low field magnetoresistance at room temperature is far from being technologically viable.

Keywords: manganites, magnetoresistance, lattice mismatch, lanthanum manganate, strain, microwaves, annealing

1. Introduction

Manganites of the form $A_{1-x}B_xMnO_3$, where A is a trivalent ion (La, Nd, Pr) and B is a divalent ion (Ba, Ca, Sr), have attracted considerable attention due to their exhibition of colossal magnetoresistance (CMR) [1–5]. A magnetoresistance $(MR = [\{\rho(H) - \rho(0)\}/\rho(0)]^*100)$ of $> -99.9\%$ has been observed in $Nd_{0.7}Sr_{0.3}MnO_{3-\delta}$ [4] at 60 K and 8 T and in semiconducting $La_{1-x}Ca_x MnO_3$ [5]. These materials offer exciting possibilities for technological applications, including magnetic sensors [6,7], such as hard disk drive read heads [8,9]. Another interesting application would be the incorporation of these materials into microwave sensors, such as modulators, based on their magnetoresistive response in the microwave regime. However, to be technologically useful in any frequency regime, the magnetoresistance values need to be large for small applied magnetic fields and the devices have to be operational at room temperature [8,9].

One approach that has been explored in the literature to achieve enhanced low field magnetoresistance is the introduction of extrinsic effects, such as grain boundaries. Bulk polycrystalline CMR manganites show an enhanced magnetoresistance at low magnetic fields [10,11]. Magnetoresistance values as high as 45% have been achieved in fields as low as 2000 Oe in $La_{0.7}Sr_{0.3}MnO_3$ [11]. However, this large

[1]Present address Department of Physics, California State University, Long Beach, 1250 Bellflower Blvd., Long Beach, CA 90840-3901.
[2]Present address Department of Chemistry and Physics, Rowan University, Glassboro, NJ 08028.
[3]Also at Department of Electrical Engineering, University of Maryland, College Park, MD 20742.
[4]Also at Department of Nuclear and Materials Engineering, University of Maryland, College Park, MD 20742.

magnetoresistance is displayed at low temperatures. Spin dependent tunneling through the grain boundary [12] and spin dependent scattering at the spin-disordered grain boundary [13] are a couple of theories that are being used to explain the low field magnetoresistance. In addition to the magnetoresistance measurements in the dc regime, 3 μm polycrystalline powders of $La_{0.7}Ba_{0.3}MnO_3$ and $La_{0.7}Sr_{0.3}MnO_3$ have been measured at microwave frequencies [14,15]. A microwave magnetoimpedance of nearly 80% at 600 Oe and at room temperature has been observed in the $La_{0.7}Ba_{0.3}MnO_3$ powder, while the $La_{0.7}Sr_{0.3}MnO_3$ powder has shown a microwave magnetoimpedance greater than 50% at 600 Oe and at room temperature [14,15]. This effect is due to the frequency dependent dynamic permeability of these conducting ferromagnets [14,15].

Using the bulk materials as an example, the effect of grain boundaries in thin films is also being explored. Recent work on coherent and incoherent grain boundaries in $La_{0.7}Sr_{0.3}MnO_3$ has shown enhanced low field MR effects at low temperatures and at room temperature [16]. However, the room temperature enhancement is minimal. Also, $La_{0.7}Sr_{0.3}MnO_3$ films, which are grown on $SrTiO_3$ bicrystals, show enhanced MR originating from the grain boundary region of the bicrystal [17–19]. A magnetoresistance of -3% at room temperature was achieved at 200 Oe and even higher values were observed at lower temperatures [19]. This result is promising, but the magnetoresistance is still not large enough for technological applications. In general, the effect of the grain boundary on the magnetoresistance is dominant only at low temperatures. Therefore, using grain boundaries to enhance the room temperature, low field magnetoresistance presents a significant challenge.

Another approach to achieving low field magnetoresistance at room temperature is field focusing. By sandwiching a single crystal $La_{0.67}Ca_{0.33}MnO_3$ (LCMO) sample between two long pieces of bulk $(Mn, Zn)Fe_2O_4$, Hwang et al. were able to obtain a room temperature magnetoresistance of -20% at 400 Oe [20]. The coercive field of the Mn-Zn ferrite is less than 1 Oe. Therefore, the stray fields from the Mn-Zn ferrite will add to the applied magnetic field to create an enhanced effective magnetic field that the LCMO will experience, thereby increasing the magnetoresistive response of the LCMO at lower applied magnetic fields. However, this effect has not been reproduced in thin films, which are more relevant for technological applications. In a similar manner, $Nd_{0.7}Sr_{0.3}MnO_3$ (NSMO) has been integrated with superconducting $YBa_2Cu_3O_7$ (YBCO) flux-focusing devices [21]. When a magnetic field is applied to a superconductor, the superconductor will try to expel the magnetic field. Therefore, by placing YBCO pads or washers around a small region of NSMO, the expulsion of the magnetic field by YBCO when a magnetic field is applied will cause the magnetic field to focus into the small NSMO region. This field focusing has shown -11% MR in the NSMO at 200 Oe and 77 K. The problem with this device is that the operational temperature of the device must be below the superconducting transition temperature of YBCO. Therefore, room temperature operation of such a device is not possible. Due to the temperature restrictions of the grain boundary and flux-focusing approaches, this work has concentrated on optimizing the intrinsic room temperature CMR effect, which exhibits a narrow peak close to the resistivity peak temperature of the CMR material.

Operation of a device based on the CMR manganites at room temperature requires that the peak magnetoresistance coincide with room temperature. Therefore, the resistivity peak temperature, T_p, of the manganite, where the paramagnetic insulator to ferromagnetic metal transition happens, must occur above room temperature, since the magnetoresistance peaks at a temperature slightly below T_p in epitaxial thin films [1–5]. This restriction on T_p limits the compositional choice in the manganite family to $La_{0.7}Ba_{0.3}MnO_3$ (LBMO) with a bulk T_p of 340 K [10] and $La_{0.7}Sr_{0.3}MnO_3$ (LSMO) with a bulk T_p of 370 K [22]. In the present work, LBMO was studied rather than LSMO due to the closer proximity of LBMO's T_p to room temperature.

In this paper, we examine the viability of single layer colossal magnetoresistance thin films for technological applications. Specifically, we studied the magnetoresistive response of $La_{0.7}Ba_{0.3}MnO_3$ (LBMO) at small applied magnetic fields and at room temperature as a function of the lattice mismatch strain and the sensing frequency. We examined the lattice mismatch strain by varying the thickness of the LBMO film, as well as by annealing the film in oxygen and using a lattice matched $SrTiO_3$ buffer layer. Also, we changed the frequency regime by measuring the magnetoresistance of the films in a

microwave cavity. We altered the frequency regime in order to deduce part of the frequency dependence of the magnetoresistance and to determine if a higher frequency would improve the magnetoresistive properties of the films.

2. Experiment

The samples used for this study were single layer LBMO thin films fabricated using pulsed laser deposition. All films were grown on (00*l*) oriented single crystal $LaAlO_3$ (LAO) substrates. The laser energy density on the target was $\sim 2\,J/cm^2$. The oxygen pressure during deposition was 400 mTorr. In order to oxygenate the samples, the oxygen pressure was increased to 760 Torr during the cool-down process (10°C/min). The substrate temperature during deposition, T_s, was varied from 650 to 820°C. The LBMO thin films varied in thickness from 400 to 1600 Å as determined by Rutherford Back Scattering and Dektak profilometry. Half of the 1000 Å film was measured as-grown, while the other half was annealed in flowing oxygen at 900°C for 1 h before measurement in order to determine the effect of oxygen annealing on the lattice mismatch strain and the MR.

Single layer LBMO films grown directly on LAO substrate experience a compressive stress due to the 3.1% difference in the LBMO and LAO bulk lattice constants, 3.91 Å and 3.79 Å, respectively. To eliminate this compressive stress, we introduced a buffer layer that is lattice matched to the LBMO film. The buffer layer, if grown thick enough, will absorb the substrate-film stress and relax to its bulk value, thereby creating a lattice matched seed layer for the LBMO film. The buffer that we utilized was $SrTiO_3$ (STO, $a = 3.905$ Å), which has a 0.13% compressive lattice mismatch with LBMO. Therefore, we grew 300 Å STO / 1000 Å LBMO / 1000 Å STO / LAO. The top layer of STO was deposited in order to prevent environmental degradation [23]. This film was compared with the unbuffered films in order to determine the lattice mismatch effect on the MR.

The crystal structure and orientation of the films were analyzed by means of four-circle X-ray diffraction. In order to determine the resistivity peak temperature, the resistance was measured as a function of temperature using a standard four-probe configuration. The dc-MR $(\text{dc-MR} = [\{\rho(H) - \rho(0)\}/\rho(0)]^*100)$ was measured at and above room temperature using the standard four probe configuration with an applied magnetic field parallel to the surface of the film. Since the dc-MR response is nearly isotropic in the plane of the film [3,24], the relative orientation of the applied magnetic field with respect to the current was not monitored. The magnetic hysteresis loops were measured at room temperature with a vibrating sample magnetometer. The magnetic field was applied in the plane of the film during these measurements. Also, standard procedures were used to measure the magnetic susceptibility of the films.

The microwave MR (μ-MR) measurements were made using conventional microwave cavity techniques. The description of the microwave spectrometer has been reported previously [25]. The two cavities used in these measurements were a standard rectangular copper cavity and a cylindrical copper cavity loaded with a single crystal sapphire cylinder. This loaded cavity has also been described elsewhere [26]. The loaded cavity displayed several modes between 8.5 and 11.5 GHz, but the mode used for our measurements was ~ 9.66 GHz. This mode was chosen because it was the mode that consistently displayed the best coupling between the cavity and the sample in the available range of frequencies. The sample was placed off-axis on the flat end of the sapphire cylinder and the dc magnetic field was applied parallel to the surface of the film. For the unloaded rectangular cavity, the sample was placed entirely inside the cavity and the measurement mode was ~ 10 GHz. Again, the applied dc magnetic field was parallel to the surface of the film. In both cases, we measured the power reflected from the cavity, $P_c(H)$, as a function of the applied magnetic field while keeping the input power to the cavity constant.

Two different microwave cavities were used because there were limitations to each cavity's performance, which will be described below. First, the definition of the microwave magnetoresistance is derived from the dc magnetoresistance:

$$\text{dc-MR}(\%) = \frac{\rho(H) - \rho(0)}{\rho(0)} * 100 \qquad (1)$$

where ρ is the resistivity of the film. Now, the power reflected from the sample is $P_c(H)$–P_c^u, where $P_c(H)$ is the power reflected from the cavity with a sample (where $H = 0$ or the applied magnetic field) and P_c^u is

the power reflected from the cavity without a sample. If $\rho_{dc} > 1\,\text{m}\Omega\text{-cm}$, which is the case for LBMO, then the power reflected from the sample, $P_c(H)$–P_c^u, is proportional to the conductivity of the sample, $\sigma(H)$, depending on the applied magnetic field ($H = 0$ or the applied magnetic field) [27]. Therefore, the definition of the μ-MR is

$$\mu\text{-MR}(\%) = \frac{-\Delta P_c}{\Delta P_c + P_c(0) - P_c{}^u} * 100 \quad (2)$$

where $\Delta P_c = P_c(H) - P_c(0)$. This measurement is possible in the unloaded rectangular cavity where P_c^u is known. However, the small signal from the sample and interference from magnetic resonance put limitations on the usefulness of this cavity to measure the μ-MR. These limitations allow the magnetoresistance measurements to be made only for high magnetic fields of ~ 6000 Oe and above. In contrast, the cavity loaded with sapphire is much more sensitive to small signals allowing the magnetoresistance to be measured at lower fields. Yet, the magnet for this cavity limits the measurement to low magnetic fields of ~ 6000 Oe or lower. More importantly, for the cavity loaded with sapphire, P_c^u changes from one measurement to the next. Therefore, it is impossible to know the value of P_c^u for each measurement.

Nevertheless, since the magnetoresistive response in the microwave regime should be the same for either cavity, we can calibrate the loaded cavity by measuring the μ-MR in the unloaded rectangular cavity and in the cavity loaded with sapphire at 6000 Oe. Equating Eq. (2) for each cavity we obtain

$$\frac{-\Delta P_c}{\Delta P_c + P_c(0) - P_c^u} * 100 = \frac{-\Delta P_c^s}{\Delta P_c^s + P_c^s(0) - P_c^{u,s}} * 100 \quad (3)$$

where the superscript ''s'' refers to the cavity loaded with sapphire. Every quantity in Eq. (3) is measurable, except for $P_c^{u,s}$. Therefore, using Eq. (3) with the measured values at 6000 Oe, we can obtain $P_c^{u,s}$. P_c^u (or $P_c^{u,s}$) is a constant as a function of the applied magnetic field. Therefore, the value of $P_c^{u,s}$ found at 6000 Oe is valid over the whole magnetic field range and this allows us to evaluate the μ-MR at low magnetic fields. Therefore, to determine the whole picture of the microwave magnetoresistance and to compare it to the dc-MR, it is necessary to use both cavities: the cavity loaded with sapphire to get the shape and the changes in the reflected power at low magnetic fields *and* the unloaded rectangular cavity to calibrate the loaded cavity's magnetoresistive values.

3. Results and Discussion

Typical X-ray diffraction data for single layer LBMO films is shown in the inset of Fig. 1. The θ-2θ scan displays only (00l) oriented peaks for the LBMO and the LAO. The ϕ scans show in-plane orientation of the a- and b-axes [23]. The diffraction data indicates that the LBMO films are purely c-axis oriented and epitaxial. Figure 1 plots the typical resistivity as a function of temperature for LBMO. The resistivity peak temperature, T_p, where the paramagnetic insulator to ferromagnetic metal transition occurs, is marked with an arrow. Room temperature, RT, is also marked with an arrow. For fully oxygenated LBMO, T_p is higher than RT, as shown in Fig. 1 [10,28]. However, oxygen deficient LBMO has T_p lower than RT [10]. Also, the microwave and dc resistivities have similar temperature dependencies in the thin films, but in bulk the microwave resistivity falls off below the peak temperature more quickly than the dc resistivity [29].

As shown previously [1–5], the dc-MR displays a peak similar to the resistivity peak as a function of temperature, although the dc-MR peak occurs at a slightly lower temperature than T_p. Thus, by choosing LBMO, rather than one of the other manganese-based perovskites, T_p can be tuned so that the dc-MR peak coincides exactly with room temperature. One method of achieving this tunability is to vary the substrate

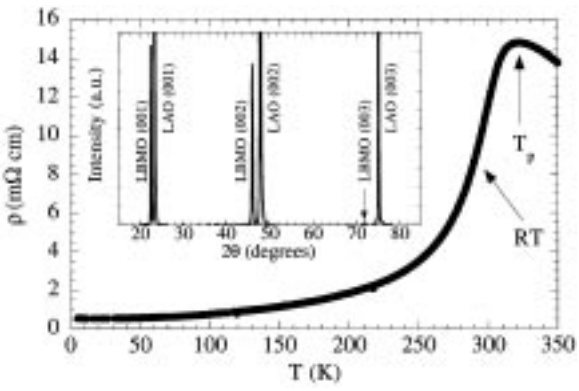

Fig. 1. Typical resistivity vs. temperature curve with the peak temperature, T_p, and room temperature, RT, marked by arrows. (Inset) Typical $\theta - 2\theta$ X-ray diffraction spectrum of single layer LBMO showing only (00l) phase peaks.

temperature during deposition, T_s. Figure 2 shows the variation of T_p with T_s for 1000 Å LBMO thin films grown in two different pulsed laser deposition chambers. The relationship is linear, in agreement with a previous report on $La_{0.7}Ca_{0.3}MnO_3$ [30]. As the substrate temperature is increased, the crystalline quality of the film improves as the film picks up more oxygen and the defect concentration in the film decreases. This increase in the substrate temperature is in fact analogous to annealing. Previous reports and data from this paper show that annealing in oxygen improves the crystalline quality of the film and increases the peak temperature [1,30]. Therefore, by varying T_s we can determine the growth conditions for maximum dc-MR at room temperature.

The typical dc-MR as a function of the applied magnetic field at room temperature is displayed in Fig. 3. Only positive magnetic fields are shown, since the magnetoresistive response is symmetric with respect to magnetic field. The response of these LBMO films to an applied magnetic field is linear. There seems to be no change in the slope of the curve as a function of the magnetic field and no hysteresis is observed. Figure 4 shows the room temperature dc-MR as a function of T_p at 500 Oe for 1000 Å LBMO thin films. A broad dip is observed in the data. The best room temperature dc-MR at 500 Oe is -1.44% in the films that have a T_p between 321 and 324 K. This range of peak temperatures for maximum dc-MR at room temperature is reproducible for other field values, confirming the linear functional form of the dc-MR with magnetic field. Another way to look at this data, which is more illuminating from the technological point of view, is to plot the field required to achieve -1% dc-MR at room temperature

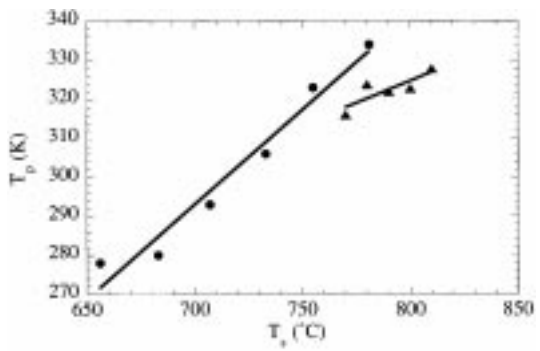

Fig. 2. Peak temperature, T_p, as a function of the substrate temperature during growth, T_s, for 1000 Å LBMO films grown in two different deposition chambers.

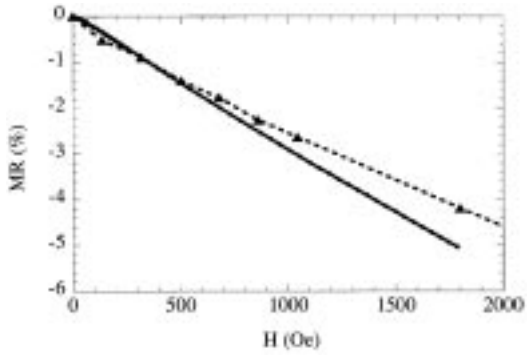

Fig. 3. Room temperature dc-MR (•) and μ-MR (▲) as a function of the applied magnetic field for a 1000 Å LBMO film.

as a function of T_p. The data presented in this manner is shown in Fig. 5. Again, there is a broad dip with the smallest required magnetic field to achieve -1% dc-MR at room temperature of 300–400 Oe occurring for peak temperatures between 321 and 324 K. These magnetic field values are among the lowest that have been reported, but are still orders of magnitude higher than those required for viable technological applications.

Microwave magnetoresistance (μ-MR) was also measured on the same set of films to determine the effect of the frequency on the magnetoresistive properties and to examine the frequency dependence of the magnetoresistance. Typical μ-MR as a function of the magnetic field is shown in Fig. 3. Only data for the positive magnetic field direction is presented, since driving the current through the magnet in the reverse direction without disturbing the sample was not possible. The response to the applied magnetic field is again linear with no obvious hysteresis. A

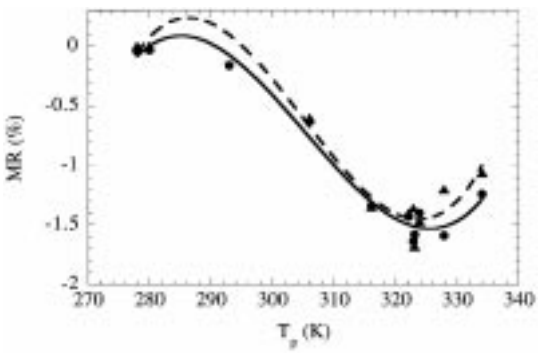

Fig. 4. Room temperature dc-MR (•) and μ-MR (▲) at 500 Oe, as a function of the peak temperature, T_p for 1000 Å LBMO films. The solid and dashed lines through the data are simply a guide to the eye.

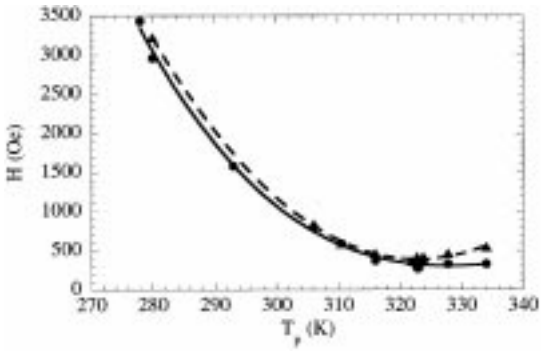

Fig. 5. Magnetic field required to achieve -1% dc-MR (•) and μ-MR (▲) at room temperature as a function of the peak temperature, T_p, for 1000 Å LBMO films. The solid and dashed lines through the data are simply a guide to the eye.

previous report on a LBMO thin film showed a change in the slope for the μ-MR at approximately 100 Oe, while the dc-MR showed no change [26]. The limited sensitivity of the present experimental set-up prevented us from looking at the μ-MR below 100 Oe, so it is impossible for us to judge the behavior in this very low field region. However, the linear behavior above 100 Oe is in agreement with the previous report [26].

Figure 4 shows the dependence of the room temperature μ-MR on T_p in an applied magnetic field of 500 Oe for 1000 Å LBMO thin films. The μ-MR shows a broad dip in its magnetoresistive response at room temperature as a function of T_p. This dip occurs between 321 and 324 K with a magnetoresistive value of -1.4%. Also, this peak is reproducible for other field values, indicating that the magnetoresistive response is linear in the microwave regime. The peak temperatures at which the maximum room temperature magnetoresistance occurs in the dc and microwave regimes are identical, as well as the magnetoresistive values at 500 Oe being the same. This equivalency of the dc- and μ-MR indicates the good, homogeneous quality of the thin films [29]. We also present the alternative plot of the magnetic field required to achieve -1% μ-MR at room temperature as a function of T_p in Fig. 5. Just as in the case for achieving -1% dc-MR, there is a broad peak around 321–324 K. The required magnetic field values are between 300 and 400 Oe. Therefore, through microwave frequencies, the sensing frequency shows no effect on the magnetoresistance of epitaxial single layer LBMO thin films.

As we have shown in Fig. 4, films that exhibit peak temperatures between 321 and 324 K show maximum magnetoresistance at room temperature. Therefore, from Fig. 2 we can see that the optimum deposition temperature is 790°C. Using this information allows us to look at the role of lattice mismatch strain on the room temperature magnetoresistance for LBMO films grown under the pre-determined optimum conditions. Therefore, a series of films with thicknesses between 400 and 1600 Å were grown at $T_s = 790$°C. Figure 6 shows the *c*-axis lattice constant as a function of the LBMO thickness. The bulk lattice constant for LBMO is 3.91 Å, while the LAO substrate has a lattice constant of 3.79 Å. Thus, there is a compressive stress in the *a–b* plane of LBMO, leading to a lengthening of the *c*-axis lattice constant as shown in Fig. 6. The *c*-axis lattice constant for LBMO is greater than the bulk value for all thicknesses studied. As the LBMO thickness increases, the *a*- and *b*-axis lattice constants begin to relax to their bulk value, which leads to a decrease of the *c*-axis lattice constant [31]. This decrease of the *c*-axis lattice constant for LBMO as the thickness increases can be seen in Fig. 6 for films that are thinner than 1000 Å. However, beyond 1000 Å, there is no longer any decrease in the *c*-axis lattice constant possibly due to the density of misfit dislocations or the presence of oxygen vacancies, which distort the LBMO unit cell and thereby affect the *c*-axis lattice constant.

Even with the partial release of the lattice mismatch strain for thicker films, the *c*-axis lattice constant for LBMO is greater than the bulk value, indicating strain in the film, which affects the magnetoresistance. Therefore, two different

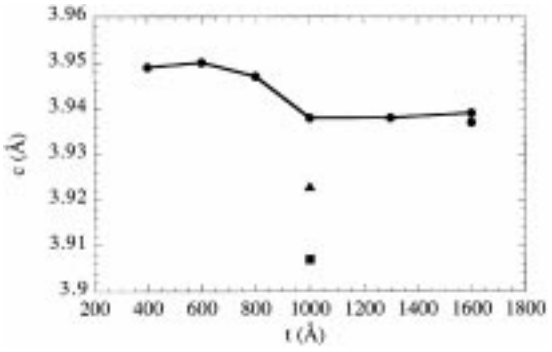

Fig. 6. The *c*-axis lattice constant, *c*, as a function of the LBMO thickness for films grown at $T_s = 790$°C (•). The *c*-axis lattice constant is also shown for 1000 Å films annealed in O_2 at 900°C for 1 h. (▲) and 1000 Å buffered films (■).

approaches were taken to further reduce the *c*-axis lattice constant. Half of the 1000 Å as-grown film was annealed at 900°C in flowing O_2 for 1 h in order to further oxygenate the film and to release the lattice mismatch strain. The lattice constant for the annealed film is also shown in Fig. 6. Upon annealing, which reduces the number of oxygen vacancies and releases the lattice mismatch strain, the *a*- and *b*-axis lattice constants for LBMO relax further towards bulk values, resulting in a further drop of the *c*-axis lattice constant [31]. For the 1000 Å LBMO film, the *c*-axis lattice constant drops from 3.938 Å to 3.924 Å. However, annealing did not provide enough release of the lattice mismatch strain to reduce the *c*-axis lattice constant to the bulk value. Hence, we looked at the second approach of introducing a lattice matched buffer layer. In this case, the buffer layer will absorb all of the lattice mismatch strain and provide a lattice matched seed layer for the LBMO film. In our case, we chose STO as the buffer layer. STO has a *c*-axis lattice constant of 3.905 Å, which is only 0.13% different from the LBMO bulk value. Figure 6 shows the *c*-axis lattice constant for a 1000 Å LBMO film grown on a STO buffer layer. The LBMO lattice constant is reduced to 3.906 Å, which is equivalent to the STO bulk lattice constant and only slightly lower than the bulk LBMO value. Thus, the STO buffer layer provides the most strain free LBMO film. We now examined the effect of the lattice mismatch strain on several other physical properties of the films.

Figure 7 shows the resistivity peak temperature, T_p, as a function of thickness for the as-grown LBMO films. For these as-grown films, the resistivity peak temperature increases as the thickness increases up to 1000 Å. After 1000 Å the resistivity peak temperature is saturated. This is in agreement with the *c*-axis lattice constant shown in Fig. 6. As the lattice mismatch strain is relaxed, the resistivity peak temperature increases. When the *c*-axis lattice constant saturates, the resistivity peak temperature saturates. This increase in the resistivity peak temperature could be due to the Mn-O-Mn bond angle approaching 180° as the lattice mismatch strain is relaxed, which increases the transfer integral for electron hopping in the double exchange model [32–36]. Compression of the film lattice to match with the substrate will subsequently cause the Mn-O-Mn bond angle to bend away from 180°. As the compression is released, the bond angle will again approach 180° and electrons will be transferred more easily from the

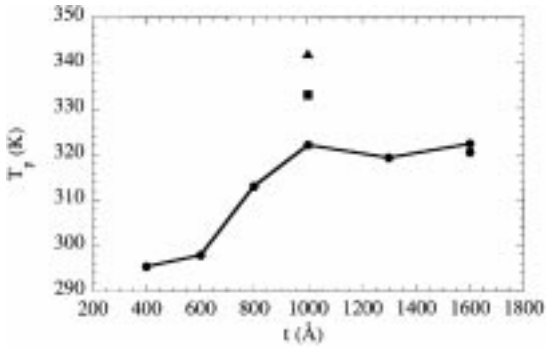

Fig. 7. The peak temperature, T_p, as a function of the LBMO thickness for films grown at $T_s = 790$°C (●). The peak temperature is also shown for 1000 Å films annealed in O_2 at 900°C for 1 h. (▲) and 1000 Å buffered films (■).

Mn^{3+} ion to the Mn^{4+} ion at higher temperatures [33–36]. In terms of room temperature magnetoresistance, the films that are thicker than 1000 Å show the appropriate resistivity peak temperature to maximize the room temperature magnetoresistive response.

The resistivity peak temperatures, for the annealed and buffered 1000 Å LBMO films, are also shown in Fig. 7. Annealing LBMO in oxygen causes the resistivity peak temperature to shift to 342 K, as expected from bulk LBMO experiments [10] and similar experiments on $La_{0.7}Ca_{0.3}MnO_3$ thin films [30], while the introduction of a lattice matched buffer layer causes the resistivity peak temperature to shift to 333 K. The increase in the resistivity peak temperatures for the annealed and buffered LBMO films again corresponds to the decrease of the *c*-axis lattice constant, as seen in Fig. 6. However, the annealed film displays a larger increase in the resistivity peak temperature despite the smaller degree of lattice mismatch relaxation observed. While the resistivity peak temperature shifts towards the bulk value with the relaxation of the lattice mismatch strain, there is the complicating issue of the number of oxygen vacancies in the films which affects the lattice constant and the resistivity peak temperature. The buffered film is not annealed, indicating that these films should have the same number of oxygen defects as the as-grown single layer films. Annealing in oxygen eliminates a high percentage of the oxygen vacancies in the LBMO thin films [1,30], in analogy with the results observed in bulk LBMO [10]. The absence of oxygen is a greater detriment to metallic conduction than a strained Mn-O-Mn bond according to the double exchange mechanism introduced by

Zener to explain conduction in the manganite materials [32]. Therefore, oxygen deficiencies will suppress the resistivity peak temperature, indicating the onset of metallic conduction in the film, further than bent Mn-O-Mn bonds. Therefore, the annealed film, with lower oxygen defect concentrations, has a higher resistivity peak temperature than the buffered film. However, both the annealed and buffered LBMO films are of higher quality than the as-grown single layer LBMO films as shown by the closer proximity of their physical properties to bulk values. Despite the superior quality of the annealed film, the resistivity peak temperature is too high to see maximum room temperature magnetoresistance. The buffered film on the other hand has a resistivity peak temperature that is consistent with maximum room temperature magnetoresistance.

In-plane magnetic hysteresis loops were also measured at room temperature. Figure 8 shows the loops for the as-grown films. Only three of the thicknesses (400 Å, 1000 Å, and 1600 Å) are shown in the graph. The 600 Å film is equivalent to the 400 Å film and the 800 Å and 1300 Å films are equivalent to the 1000 Å film. The 400 Å film shows paramagnetic behavior at room temperature, which is consistent with a resistivity peak temperature of 295 K. The 1000 Å and 1600 Å films are ferromagnetic with a coercive field of 14 Oe. The 1600 Å film has an enhanced in-plane magnetic susceptibility and a higher saturation magnetization compared to the 1000 Å film, although both have $\chi < 30$, which is the sensitivity limit of the measurement set-up for the magnetic susceptibility. The enhancement of the in-plane magnetic susceptibility and saturation magnetization for the thicker as-grown LBMO films can be attributed to the orientation of the magnetic easy axis. Previous reports on $La_{0.7}Sr_{0.3}MnO_3$ and TbDyFe thin films have shown that when strain effects dominate the magnetic anisotropy, the magnetic easy axis no longer lies in the plane of the film [37,38]. In fact, for $La_{0.7}Sr_{0.3}MnO_3$ thin films grown on $LaAlO_3$ substrate, the orientation of the magnetic easy axis depends on the thin film thickness [37]. Therefore, a comparison can be drawn between these previous reports and the results for the as-grown LBMO thin films. For the thinner as-grown LBMO films, it is possible that the lattice mismatch strain dominates the magnetic anisotropy and the magnetic easy axis is at an angle, θ, with the film plane. As the lattice mismatch strain is released by growing thicker films, the angle the magnetic easy axis makes with the film plane, θ, decreases and the component of the in-plane magnetization increases. Correspondingly, the in-plane magnetic susceptibility and saturation magnetization increase.

The room temperature in-plane hysteresis loops for the as-grown, annealed, and buffered 1000 Å LBMO films are shown in Fig. 9. All three loops have the same coercive field, whereas the magnetic susceptibilities are different. The as-grown film has $\chi < 30$ as shown above, whereas the annealed film has $\chi = 280$ and the buffered film has $\chi = 30 - 300$ depending on the particular film. The increase in the magnetic susceptibility for the annealed and buffered films reflects both the decrease of the angle, θ, that the magnetic easy axis makes with the plane of the film [37,38] and the increase of the magnetic homogeneity in these films with the decrease of the lattice mismatch

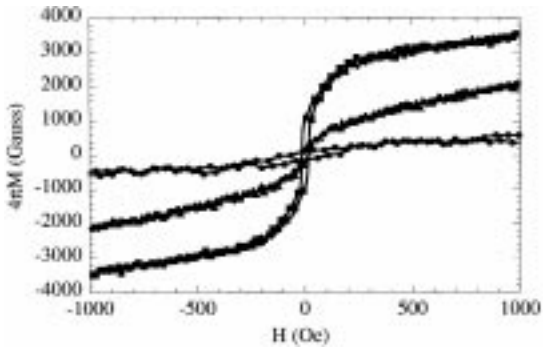

Fig. 8. Magnetic hysteresis loops for various LBMO thicknesses (● = 400 Å, ▲ = 1000 Å, ■ = 1600 Å) for films grown at $T_s = 790°C$.

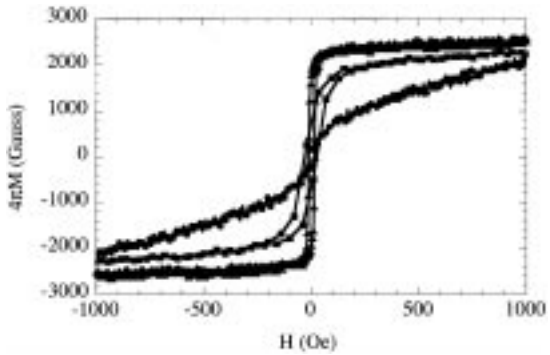

Fig. 9. Magnetic hysteresis loops for the as-grown single layer film (●), the annealed film (▲), and the buffered film (■) with the LBMO thickness at 1000 Å and $T_s = 790°C$.

strain. Despite the fact that the buffered film is the most relaxed and should have the largest susceptibility and saturation magnetization, the annealed film shows a higher saturation magnetization due to the lower density of oxygen vacancies that occur after O_2 annealing compared to as-grown films (buffered or not).

Figure 10 plots the magnetoresistance at 500 Oe as a function of the thickness of the LBMO films. The films that are less than or equal to 600 Å were measured at room temperature, which corresponds to 0.99 T_p. The 800 Å film was measured at room temperature or 0.92 T_p and the films thicker than 800 Å were measured at room temperature or 0.9 T_p (the temperature at which maximum magnetoresistance occurs). Figure 4 showed that the maximum dc-MR occurred at a temperature that is nine-tenths of the resistivity peak temperature. Therefore, the films that are thicker than 800 Å show room temperature being equivalent to the temperature for maximum dc-MR and these are the films that are most promising for technological applications. The dc-MR shows a roughly linear increase with the film thickness. This increase in dc-MR corresponds to the release of the lattice mismatch strain and the improved in-plane magnetic homogeneity of the samples as the thickness increases. For maximum dc-MR at room temperature the 1600 Å film is the best, but -1.7% MR at 500 Oe is too small for technological applications.

The dc-MR for the annealed and buffered films measured at 0.9 $T_p = 309$ K and 0.89 $T_p =$ room temperature, respectively, are also shown in Fig. 10 for an applied magnetic field of 500 Oe. The dc-MR values for these films are greater than those for the as-grown films. In fact, the annealed film shows the best dc-MR of -1.9% at 500 Oe. We suspect that the improved dc-MR values for the annealed and buffered films are again related to the decrease of oxygen vacancies, the elimination of lattice mismatch strain, and the improved magnetic homogeneity of the films. In addition, the role of microstructural differences between the as-grown, annealed, and buffered LBMO films on the dc-MR must be explored, but are not considered here. Figure 11 shows the as-grown, annealed, and trilayer dc-MR at 0.9 T_p as a function of the applied magnetic field for 1000 Å LBMO films. The annealed films show an enhanced dc-MR at low magnetic fields compared to the as-grown single layer and buffered films. The origin of this enhancement at low magnetic fields is still under investigation. However, the magnetoresistance values obtained at 500 Oe in these improved films are still too small to be technologically viable.

In an effort to look at this data from the technological viewpoint, we have graphed the magnetic field required to achieve -1% dc-MR as a function of thickness for the as-grown, annealed, and buffered films in Fig. 12. The magnetic field required to achieve -1% dc-MR reaches a minimum of 280 Oe at 1600 Å for the as-grown films. The buffered LBMO film equals this minimum magnetic field of 280 Oe to reach -1% dc-MR at room temperature. The annealed film shows lower minimum magnetic fields, i.e., 225 Oe, but they are

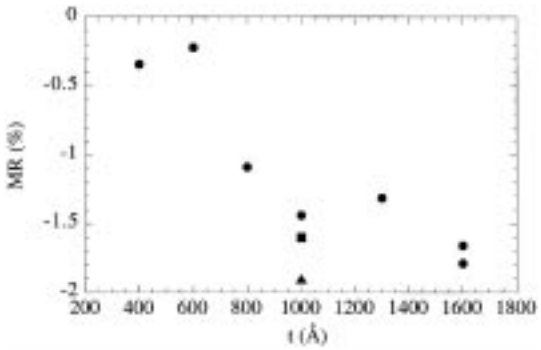

Fig. 10. Magnetoresistance at 500 Oe as a function of the LBMO thickness for films grown at $T_s = 790°C$ (●). The 400 and 600 Å films were measured at 0.99 T_p, whereas the others were measured at 0.9–0.92 T_p. The magnetoresistance at 500 Oe is also shown for 1000 Å films annealed in O_2 at 900°C for 1 h. (▲) and 1000 Å buffered films (■).

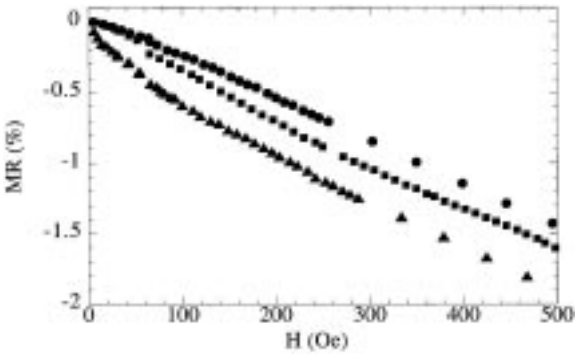

Fig. 11. DC-MR as a function of magnetic field for the as-grown single layer film (●), the annealed film (▲), and the buffered film (■) with the LBMO thickness at 1000 Å and $T_s = 790°C$.

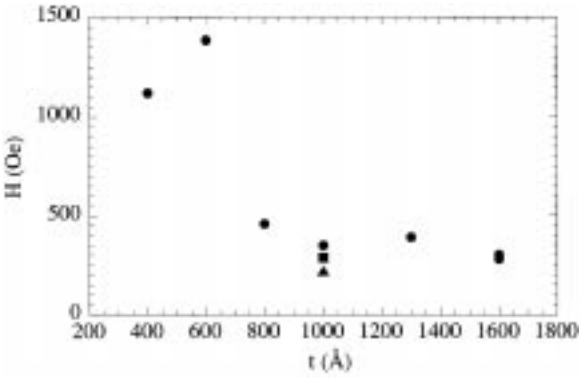

Fig. 12. Magnetic field required to achieve -1% dc-MR at room temperature as a function of the LBMO film thickness for the as-grown films (●). The values for the annealed film (▲) and the buffered film (■) are also shown.

reached at temperatures above room temperature. From this alternative viewpoint it is evident that the magnetic fields required to achieve -1% magnetoresistance for all the films studied in this paper are too large for implementation in technological applications.

4. Conclusions

In summary, we have shown that microwave frequencies do not enhance the magnetoresistive response of LBMO single layer thin films over the dc-MR. Also, a 1600 Å LBMO as-grown film with a T_p between 321 and 324 K and a 1000 Å LBMO film buffered with STO yields the maximum dc and microwave magnetoresistive response at room temperature. The annealed film shows even greater maximum dc magnetoresistance, but the maximum is reached at a temperature greater than room temperature. Despite the optimization of the films presented in this paper using thickness, oxygen annealing, and buffer layers as parameters, the dc-MR values obtained are still too small at low magnetic fields and room temperature to be technologically applicable. Therefore, current attention has shifted to solving the challenge of observing grain boundary magnetoresistance effects at room temperature in granular films, to continue exploring the idea of field focusing in thin films, and to developing heterostructures, such as spin tunneling devices, spin valves, and multilayers.

The present work is supported by the Office of Naval Research under Grant No. ONR-N000149510547. M. C. Robson would also like to acknowledge J. Y. Gu, K.-C. Kim, and R. P. Sharma for their helpful contributions to the completion of this work.

References

1. R. von Helmholt, J. Wecker, B. Holzapfel, L. Schultz, and K. Samwer, *Phys. Rev. Lett.*, **71**, 2331 (1993).
2. S. Jin, T.H. Tiefel, M. McCormack, R.A. Fastnacht, R. Ramesh, and L.H. Chen, *Science*, **264**, 413 (1994).
3. H.L. Ju, C. Kwon, Q. Li, R.L. Greene, and T. Venkatesan, *Appl. Phys. Lett.*, **65**, 2110 (1994).
4. G.C. Xiong, Q. Li, H.L. Ju, S.N. Mao, L. Senapati, X.X. Xi, R.L. Greene, and T. Venkatesan, *Appl. Phys. Lett.*, **66**, 1427 (1995).
5. G.-Q. Gong, C. Canedy, G. Xiao, J.Z. Sun, A. Gupta, and W.J. Gallagher, *Appl. Phys. Lett.*, **67**, 1783 (1995).
6. J. Heremans, *J. Phys. D: Appl. Phys.*, **26**, 1149 (1993).
7. S. Jin, M. McCormack, T.H. Tiefel, and R. Ramesh, *J. Appl. Phys.*, **76**, 6929 (1994).
8. K. Derbyshire and E. Korczynski, *Solid State Technology*, 57 (1995).
9. James A. Brug, Thomas C. Anthony, and Janice H. Nickel, *MRS Bulletin*, 23 (1996).
10. H.L. Ju, J. Gopalakrishnan, J.L. Peng, Qi Li, G.C. Xiong, T. Venkatesan, and R.L. Greene, *Phys. Rev.*, **B51**, 6143 (1995).
11. P. Schiffer, A.P. Ramirez, W. Bao, and S.-W. Cheong, *Phys. Rev.*, **B75**, 3336 (1995).
12. H.Y. Hwang, S.-W. Cheong, N.P. Ong, and B. Batlogg, *Phys. Rev. Lett.*, **77**, 2041 (1996).
13. A. Gupta, G.Q. Gong, Gang Xiao, P.R. Duncombe, P. Lecoeur, P. Trouilloud, Y.Y. Wang, V.P. Dravid, and J.Z. Sun, *Phys. Rev.*, **B54**, R15629 (1996).
14. V.V. Srinivasu, S.E. Lofland, and S.M. Bhagat, *J. Appl. Phys.*, **83**, 2866 (1998).
15. V.V. Srinivasu, S.E. Lofland, S.M. Bhagat, K. Ghosh, and S.D. Tyagi, *J. Appl. Phys.*, **86**, 1067 (1999).
16. J.Y. Gu, S.B. Ogale, M. Rajeswari, T. Venkatesan, R. Ramesh, V. Radmilovic, U. Dahmen, G. Thomas, and T.W. Noh, *Appl. Phys. Lett.*, **72**, 1113 (1998).
17. K. Steenbeck, T. Eick, K. Kirsch, K. O'Donnell, and E. Steinbeib, *Appl. Phys. Lett.*, **71**, 968 (1997).
18. N.D. Mathur, G. Burnell, S.P. Isaac, T.J. Jackson, B.-S. Teo, J.L. MacManus-Driscoll, L.F. Cohen, J.E. Evetts, and M.G. Blamire, *Nature*, **387**, 266 (1997).
19. S.P. Isaac, N.D. Mathur, J.E. Evetts, and M.B. Blamire, *Appl. Phys. Lett.*, **72**, 2038 (1998).
20. H.Y. Hwang, S.-W. Cheong, and B. Batlogg, *Appl. Phys. Lett.*, **68**, 3494 (1996).
21. Z.W. Dong, T. Boettcher, C.-H. Chen, I. Takeuchi, M. Rajeswari, R.P. Sharma, and T. Venkatesan, *Appl. Phys. Lett.*, **69**, 3432 (1996).
22. A. Urushibara, Y. Moritomo, T. Arima, A. Asamitsu, G. Kido, and Y. Tokura, *Phys. Rev.*, **B51**, 14103 (1995).

23. M.C. Robson, C. Kwon, K.-C. Kim, R.P. Sharma, T. Venkatesan, R. Ramesh, S.E. Lofland, M. Dominguez, S.D. Tyagi, and S.M. Bhagat, *J. Appl. Phys*., **80**, 2334 (1996).
24. J. Volger, *Physica*, **20**, 49 (1951).
25. S.M. Bhagat, *Techniques of Metal Research*, ed. by E. Passaglia (Interscience, New York, 1974), Vol. VI, Part 2, Ch. 8.
26. S.D. Tyagi, S.E. Lofland, M. Dominguez, S.M. Bhagat, C. Kwon, M.C. Robson, R. Ramesh, and T. Venkatesan, *Appl. Phys. Lett*., **68**, 2893 (1996).
27. S.E. Lofland, M. Dominguez, S.D. Tyagi, S.M. Bhagat, M.C. Robson, C. Kwon, Z. Trajanovic, I. Takeuchi, R. Ramesh, and T. Venkatesan, *Thin Solid Films*, **288**, 256 (1996).
28. R. von Helmolt, J. Wecker, K. Samwer, L. Haupt, and K. Bärner, *J. Appl. Phys*., **76**, 6925 (1994).
29. M. Dominguez, S.M. Bhagat, S.E. Lofland, J.S. Ramachandran, G.C. Xiong, H.L. Ju, T. Venkatesan, and R.L. Greene, *Europhys. Lett*., **32**, 349 (1995).
30. A. Goyal, M. Rajeswari, R. Shreekala, S.E. Lofland, S.M.Bhagat, T. Boettcher, C. Kwon, R. Ramesh, and T. Venkatesan, *Appl. Phys. Lett*., **17**, 2535 (1997).
31. M. Ohring, *The Materials Science of Thin Films* (Academic Press, Inc., San Diego, 1992), Ch. 7.
32. C. Zener, *Phys. Rev*., **82**, 403 (1951).
33. H.Y. Hwang, S.-W. Cheong, P.G. Radaelli, N. Marezio, and B. Batlogg, *Phys. Rev. Lett*., **75**, 914 (1995).
34. J. Fontcuberta, B. Martinez, A. Seffar, S. Pinol, J.L. Garcia-Munoz, and X. Obradors, *Phys*., **76**, 1122 (1996).
35. M.R. Ibarra, P.A. Algarabel, C. Marquina, J. Blasco, and J. Garcia, *Phys. Rev. Lett*., **75**, 3541 (1995).
36. H.Y. Hwang, T.T.M. Palstra, S.-W. Cheong, and B. Batlogg, *Phys. Rev*., **B52**, 15046 (1995).
37. C. Kwon, K.-C. Kim, M.C. Robson, S.E. Lofland, S.M. Bhagat, T. Venkatesan, R. Ramesh, and R.D. Gomez, *J. Magn. Magn. Mater*., **172**, 229 (1996).
38. F. Schatz, M. Hirscher, M. Schnell, G. Flik, and H. Kronmuller, *J. Appl. Phys*., **76**, 5380 (1994).